



Supporting Online Material for
**Homogeneous Distribution of ^{26}Al in the Solar System from the Mg
Isotopic Composition of Chondrules**

Johan Villeneuve,* Marc Chaussidon, Guy Libourel

*To whom correspondence should be addressed. E-mail: johanv@crpg.cnrs-nancy.fr

Published 21 August 2009, *Science* **325**, 985 (2009)
DOI: 10.1126/science.1173907

This PDF file includes:

Materials and Methods

Figs. S1 to S5

Tables S1 to S2

References

Supporting Online Material

1. Materials and Methods

1.1 Materials

Sem-Ch2 is a round PO (Porphyritic with Olivine) type I (FeO-poor) chondrule which consists of forsteritic olivine (Fo₉₇), low-Ca pyroxene (En₉₀, Wo₆, Fs₄) and Fe, Ni-metal nodules surrounded by microcrystallized mesostasis. Mesostasis is an equilibrated mix of small dendritic high-Ca pyroxenes and glass. Olivine grains are corroded and contain Fe, Ni-metal and rare melt inclusions. In the chondrule periphery, low-Ca pyroxenes form elongated grains which sometime poikilitically enclosed olivine grains.

Sem-Ch121 is a POP (Porphyritic with Olivine and Pyroxene) type I chondrule and consists of forsteritic olivine grains (Fo₉₂) and large low-Ca pyroxenes (En₈₄, Wo₆, Fs₁₀) mostly on the edge. The core of the chondrule contains small corroded olivine surrounded by large patches of glassy mesostasis with dendritic high-Ca pyroxenes. The edges of corroded olivine are mostly enclosed in low-Ca pyroxene. Fe-Ni nodules are very small and rare.

Sem-Ch32 is a PP (Porphyritic with Pyroxene) type I chondrule and exclusively contains elongated and large low-Ca pyroxenes (En₉₀, Wo₁, Fs₉) enclosed in glassy mesostasis with numerous and small dendritic high-Ca pyroxenes. Fe-Ni nodules are small and rare.

Sem-Ch21 and Sem-Ch83 are both similar PO type II (FeO-rich) chondrules and consist of large iron-rich olivines (Fo₆₅ and Fo₇₀ respectively) zoned from the core to the edge (from ~Fo₈₀ to ~Fo₅₀) which sometime poikilitically enclose relict forsteritic olivine (~Fo₉₅). Olivine grains are surrounded by a glassy mesostasis with dendritic high-Ca pyroxenes.

Sem-Ch136 is another PO type II chondrule which is probably more a clast than an entire chondrule. It contains olivine grains (Fo₉₁) surrounded by large patches of glassy mesostasis with dendritic high-Ca pyroxene.

Sem-Ch62, Sem-Ch76, Sem-Ch113 and Sem-Ch114 are POP type II chondrules which consist of large olivine (Fo₆₆, Fo₇₂, Fo₇₀ and Fo₆₄ respectively) and low-Ca pyroxene (En₄₈, Wo₆, Fs₄₅; En₅₆, Wo₁₀, Fs₃₄; En₅₂, Wo₈, Fs₄₀ and En₄₈, Wo₁₀, Fs₄₂ respectively) in similar proportions surrounded by glassy mesostasis. Low-Ca pyroxenes formed elongated grains along the chondrule edge. These chondrules contain no or few high-Ca pyroxenes. Olivine shows a zonation in Fe content from the core to the edge (from ~Fo₄₅ to ~Fo₈₀). They sometimes contain small Fe,Ni-metal nodules.

Sem-Ch137 is a POP type II chondrule which consists of a fractured overlap of iron-rich olivine (Fo₅₇), low-Ca pyroxene (En₅₀, Wo₆, and Fs₄₄), glassy mesostasis and a few plagioclases.

Sem-Ch64, Sem-Ch81 and Sem-Ch138 are PP type II chondrules which contain large euhedral low-Ca pyroxenes (En₅₇, Wo_{<1}, Fs₄₃; En₆₄, Wo₄, Fs₃₂ and En₆₀, Wo_{<1}, Fs₃₉ respectively) surrounded by glassy mesostasis for Sem-Ch138 and glassy mesostasis with small dendritic high-Ca pyroxene for Sem-Ch64 and Sem-Ch81. Fe, Ni-metal nodules are minor. Sem-Ch81 contains rare highly-corroded forsteritic olivine grains, poikilitically enclosed by low-Ca pyroxene, surrounded by glassy mesostasis with small dendritic high-Ca pyroxenes.

Sem-Ch4 is an Al-rich chondrule which mainly contains large forsteritic olivines (Fo₉₉) surrounded by large patches of mesostasis with dendritic high-Ca pyroxenes; spinel is rare. Small euhedral olivine crystals define a corona at the chondrule edge.

1.2 Methods

The Mg isotopic compositions and the Al/Mg ratios were measured at CRPG-CNRS (Nancy, France) with the Cameca ims 1270 ion microprobe. The samples were sputtered with a 30nA O⁻ primary beam of $\approx 25\mu\text{m}$ diameter. The positive secondary ions accelerated at 10kV were detected in multicollection mode using four Faraday cups (L'2 trolley for ²⁴Mg, C trolley for ²⁵Mg, H1 trolley for ²⁶Mg and H'2 trolley for ²⁷Al). One measurement consists of 40 cycles of 10 seconds counting for a total acquisition time of 400 seconds. To insure large flat top peaks, the mass resolution (M/ Δ M) was kept at the minimum possible value with the ims 1270 multicollection system, i.e. M/ Δ M = 2500 using slit number one. At this mass resolution, ²⁴MgH is not totally resolved from ²⁵Mg (M/ Δ M = 3559 between ²⁴MgH and ²⁵Mg) but high mass resolution analysis of our standards showed that with the current vacuum conditions in the sample chamber (P < 3 $\times 10^{-9}$ torr), the hydride contribution was kept negligible (< 5 $\times 10^{-6}$ of the ²⁵Mg peak intensity, i.e. corresponding to less than 0.005 ‰ on $\delta^{25}\text{Mg}$).

Stability of the backgrounds of the Faraday cups

One of the major limiting factors on the precision of the Mg isotope analyses was found to be the small variations of the backgrounds of the Faraday cups. The amplifiers were equipped with a 10¹⁰ ohm resistor for ²⁴Mg and with 10¹¹ Ohm resistors for ²⁵Mg, ²⁶Mg and ²⁷Al. The yields and the backgrounds of the four Faraday cups were determined during each analytical session with the built-in ims 1270 software. Long term variations of up to ± 5000 counts/sec (Fig. S1) for the backgrounds were observed over 10 hours. These variations, if not corrected for, would induce small but significant errors (< ± 0.04 ‰) on $\delta^{25}\text{Mg}$ measured in Mg-rich phases such as olivine (typical count rate of 1×10^9 counts/sec for ²⁴Mg) but much larger errors (< ± 1.3 ‰) in Mg-poor phases like chondrule mesostasis (typical count rate of 3×10^7 counts/sec on ²⁴Mg). Fortunately, detailed monitoring over one hour of background variations showed that short term variations, especially for ²⁵Mg and ²⁶Mg, were not random (Fig. S1) so that a precise correction could be applied for each analysis. The larger variations observed on L'2, due to the 10¹⁰ ohm resistor, were not limiting because ²⁴Mg is the most abundant isotope, i.e. the less sensitive to background variations. Thus the backgrounds on the four Faraday cups were systematically measured every 30 minutes. The values of backgrounds used to correct each analysis were determined from a linear interpolation with time made between the two nearest background measurements (2 analyses between each background analysis).

Instrumental mass fractionation

Five terrestrial standards (San Carlos olivine, Vitim olivine 313-3, Vitim orthopyroxene 313-3, CLDR01V MORB glass and BCR2-G glass) were used to calibrate instrumental mass fractionation of Mg isotopes during ion probe analysis. The instrumental mass fractionation (α) between two phases A and B can be written as an exponential law according to:

$$\alpha^{25/24}_{A/B} = (\alpha^{26/24}_{A/B})^\beta \text{ with } \alpha^{25/24}_{A/B} = ({}^{25}\text{Mg}/{}^{24}\text{Mg})_A / ({}^{25}\text{Mg}/{}^{24}\text{Mg})_B,$$

and β the exponential factor. The average Mg isotopic ratios determined on Vitim orthopyroxene during each session were taken as our reference ratios to calculate the value of α for each measurement. A value was determined for β during each analytical session from the analyses of the terrestrial standards (Fig. S2). The value of β was observed to vary from session to session from ≈ 0.505 to ≈ 0.515 , and being stable at $\approx \pm 0.002$ during one session. Many analytical parameters could explain these variations from session to session. The ^{26}Mg excesses (i.e. the deviation from the exponential mass fractionation law), noted $\Delta^{26}\text{Mg}$, are expressed in ‰ as:

$$\Delta^{26}\text{Mg} = (\alpha^{26/24} / ((\alpha^{25/24})^{1/\beta} \times \alpha^{26/24}_0) - 1) \times 1000$$

$$\text{or as: } \Delta^{26}\text{Mg} \approx \delta^{26}\text{Mg} - (1/\beta \times \delta^{25}\text{Mg} + \delta^{26}\text{Mg}_0)$$

In agreement with their terrestrial nature, the standards (olivine, pyroxene and glass taken together) showed no significant ^{26}Mg excesses with an average $\Delta^{26}\text{Mg}$ value of $0.001 \pm 0.005\text{‰}$ (2 sigma error on 62 analyses, Fig. S2). The ^{26}Mg excesses were calculated for the chondrules using the β value determined from the terrestrial standards. The two sigma internal errors on $\delta^{26}\text{Mg}^*$ (the $\Delta^{26}\text{Mg}$ due to radioactive decay of ^{26}Al) were calculated from the counting statistics on $^{25}\text{Mg}/^{24}\text{Mg}$ and $^{26}\text{Mg}/^{24}\text{Mg}$ ratios according to:

$$2\sigma_{\delta^{26}\text{Mg}^*} = 2 \times (\sigma_{\delta^{26}\text{Mg}}^2 + (1/\beta \times \sigma_{\delta^{25}\text{Mg}})^2 - 2 \times (1/\beta) \times \sigma_{\delta^{25}\text{Mg}} \times \sigma_{\delta^{26}\text{Mg}} \times \rho)^{0.5}$$

$$\text{with } \rho = \sigma_{\delta^{25}\text{Mg}}^2 + \sigma_{\delta^{26}\text{Mg}}^2 + \sigma_{\delta^{26}\text{Mg}/^{25}\text{Mg}}^2 / (2 \times \sigma_{\delta^{25}\text{Mg}} \times \sigma_{\delta^{26}\text{Mg}})$$

A typical value of 0.6 was obtained for ρ (correlation factor between $\delta^{25}\text{Mg}$ and $\delta^{26}\text{Mg}$), yielding two sigma internal errors for $\delta^{26}\text{Mg}^*$ in chondrules ranging from $\pm 0.015\text{‰}$ to $\pm 1.983\text{‰}$ (Table S1). Theoretically, the final two sigma error on $\delta^{26}\text{Mg}^*$ in chondrules is calculated by adding in quadratic way to the internal error due to counting statistics, the two sigma external error determined on the standards ($\pm 0.005\text{‰}$, Fig. S2), but this external error however is negligible in comparison to internal errors.

The non-radiogenic $\delta^{25}\text{Mg}$ variations in chondrules cannot be determined with the same high precision as that for $\delta^{26}\text{Mg}^*$ values (i.e. $\pm 0.02\text{‰}$ for olivine, see above). This is due to the fact that (i) instrumental mass fractionation varies by up to $\pm 0.5\text{‰}$ (in Vitim olivine for instance) during a given analytical session and (ii) large matrix effects exist for Mg isotopes within silicates, e.g. $\approx 5\text{‰}$ difference of instrumental mass fractionation in $\delta^{25}\text{Mg}$ between Vitim olivine and CLDR01 MORB glass (the five standards coming from fresh mantle rocks were assumed to have a $\delta^{25}\text{Mg}$ of 0‰). In addition, large matrix effects are also present in olivines depending on their Fe content (e.g. $\approx 4\text{‰}$ difference of instrumental mass fractionation in $\delta^{25}\text{Mg}$ between a Fo₁₀₀ and a Fo₇₀) and in glasses depending on their compositions. Because of the high precision of the measured $^{25}\text{Mg}/^{24}\text{Mg}$ ratios (typical 1 sigma counting statistics range from 0.006‰ to 0.6‰), a precise correction of instrumental mass fractionation in chondrules would require extremely precise calibration of matrix effects using a dedicated suite of standard minerals (olivines, pyroxenes, basaltic and synthetic glasses, ...) analyzed by MC-ICPMS. This task is in progress but is beyond the scope of the present work aimed at determining precisely ^{26}Mg excesses. Fig. S3 shows $\delta^{25}\text{Mg}$ values, corrected at first order instrumental mass fractionation, for all the data reported in Table S1. This is enough to show that none of the chondrules have significant mass fractionation effects that could be attributed to another source of fractionation (evaporation for example).

Al and Mg ion yields

Because Al and Mg have slightly different ion yields during ion probe analysis, their relative yield [yield Al/Mg = $(^{27}\text{Al}^+ / ^{24}\text{Mg}^+)_{\text{measured}} / (^{27}\text{Al} / ^{24}\text{Mg})_{\text{true}}$] must be determined precisely before any $^{26}\text{Al} / ^{27}\text{Al}$ ratios can be calculated from experimental isochrons. There are no significant matrix effects on the Al/Mg yield within our analytical precision and compositional range as shown by detailed analysis of a set of olivines, pyroxenes and glasses with variable Al/Mg ratios, i.e. $\pm 1.5\%$ of variation between the different minerals. The yields calculated from the standards of glasses, which varied from 0.73 to 0.82 (± 0.005) from session to session, were used to correct the measured $^{27}\text{Al} / ^{24}\text{Mg}$ ratios. The variations of Al/Mg yields are significant from session to session depending on the analytical settings and thus must be determined during each session. The 2 sigma errors for the $^{27}\text{Al} / ^{24}\text{Mg}$ ratios given in Table S1 are $\pm 7\%$ relative, calculated from counting statistics and the external reproducibility on the Al/Mg yield determined on the standards.

2. Supporting figures

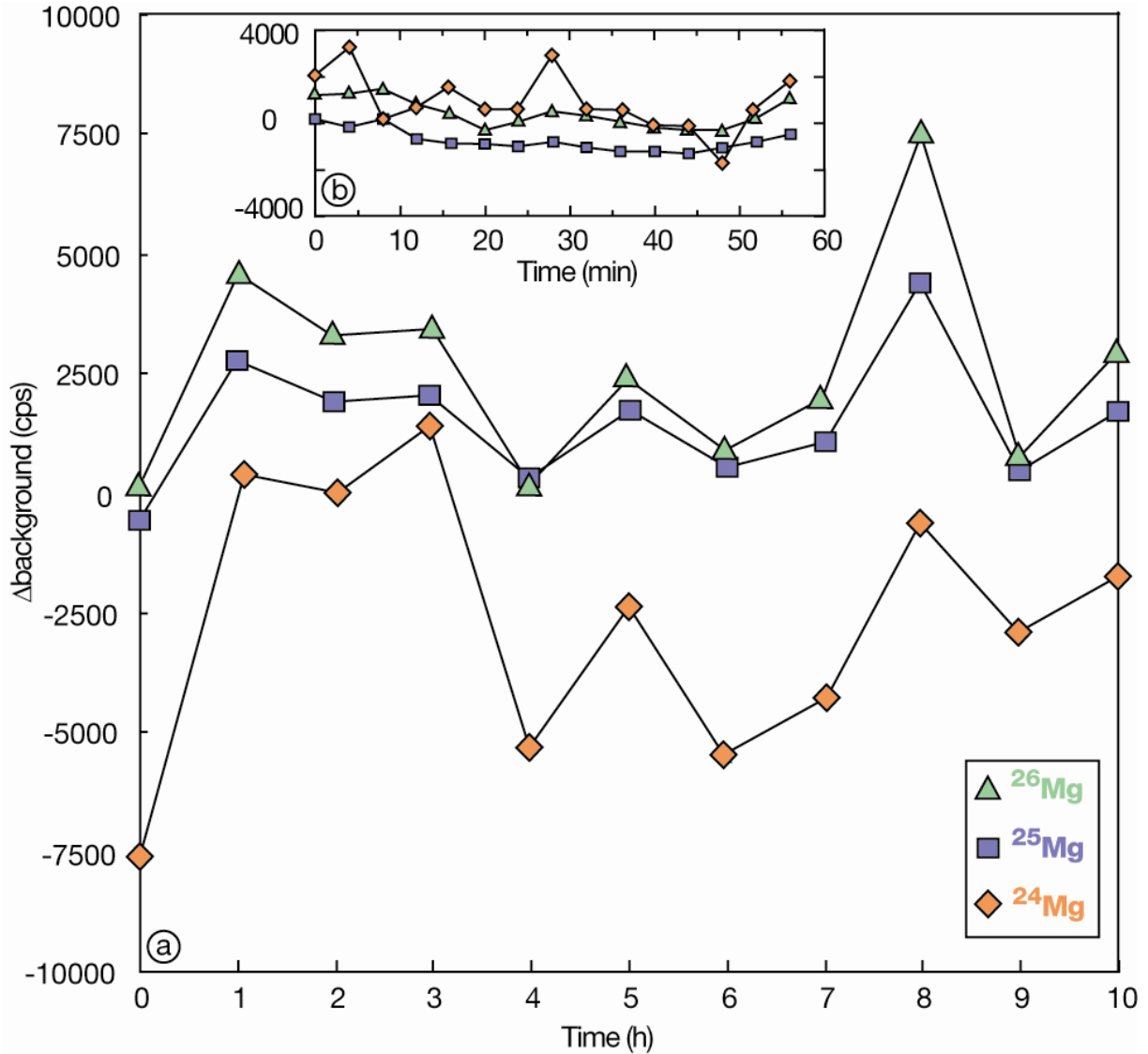


Fig. S1: a) Long term and b) short term background variations of Faraday cups L'2, C and H1 which are used for ^{24}Mg , ^{25}Mg and ^{26}Mg respectively. Each data is the difference between the measured background and the background reference value determined at the beginning of a session. The larger amplitude of the background variations on L'2 is due to the 10^{10} Ohm resistor.

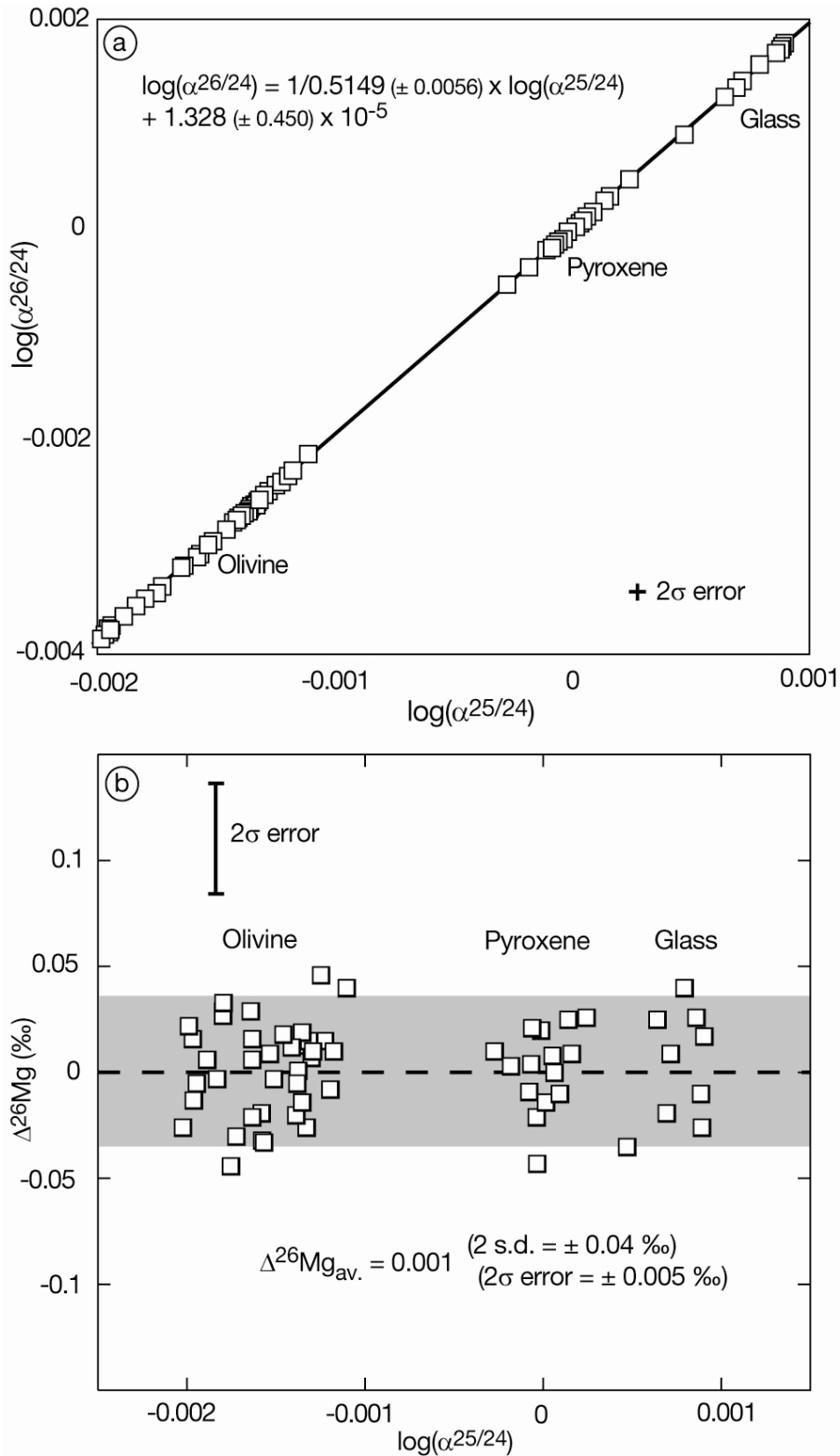


Fig. S2: **a)** An example of the instrumental mass fractionation law for the Mg isotopes obtained for a single analytical session. A very precise value of 0.5149 ± 0.0015 is calculated for β by linear regression, using Isoplot 3.0 software (S17). **b)** ^{26}Mg excesses in olivine, pyroxene and glass standards for one session, expressed as $\Delta^{26}\text{Mg} = (10^{\log \alpha^{26/24}} - (1/0.5149 \times \log \alpha^{25/24} + 0.00001328) - 1) \times 1000$. The 2σ error is calculated by dividing the standard deviation (s.d.) by the square root of the number of standards analyses during the session.

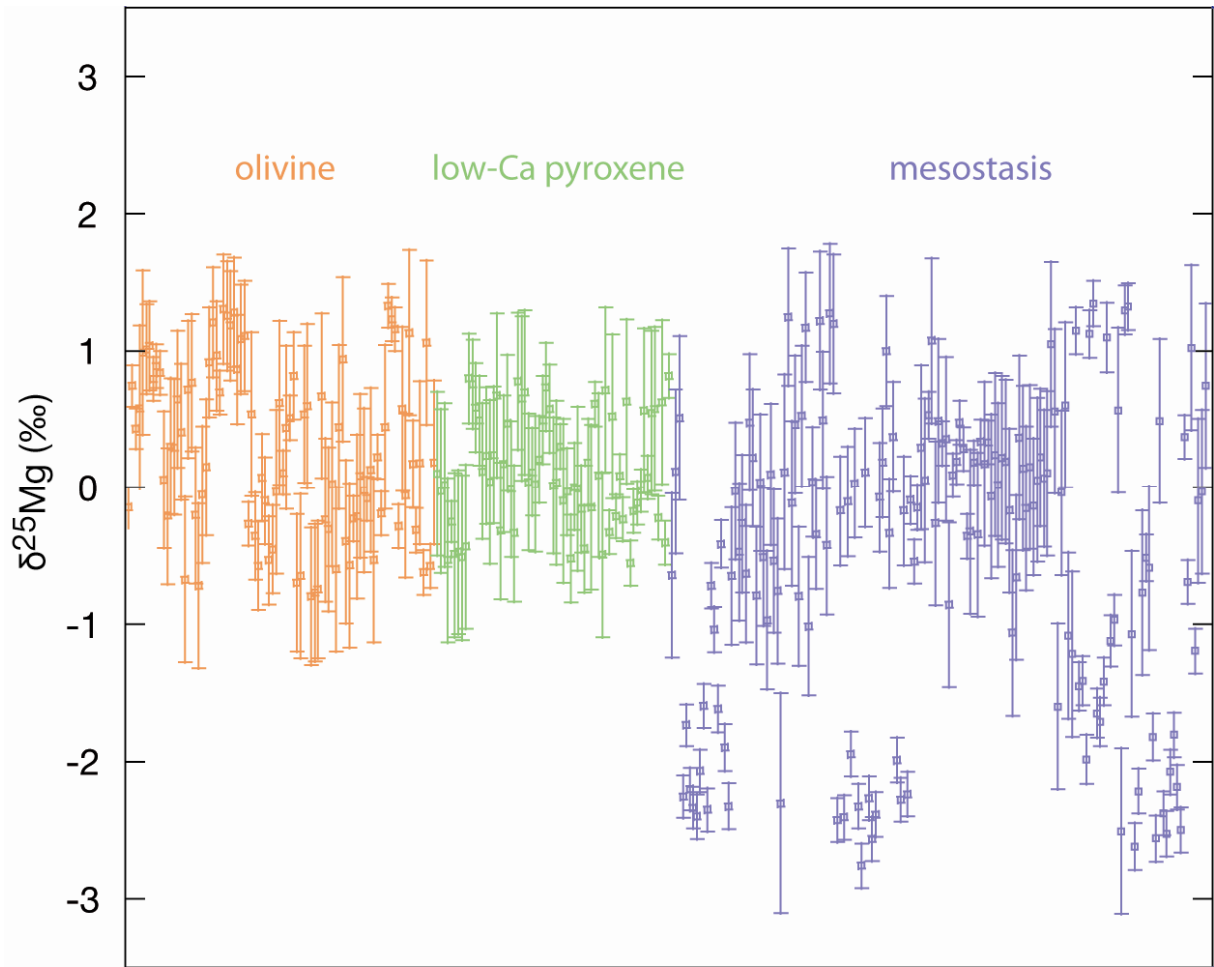
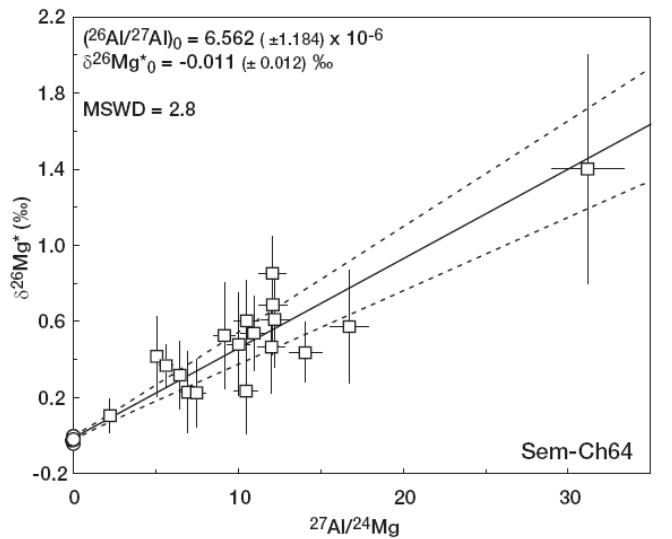
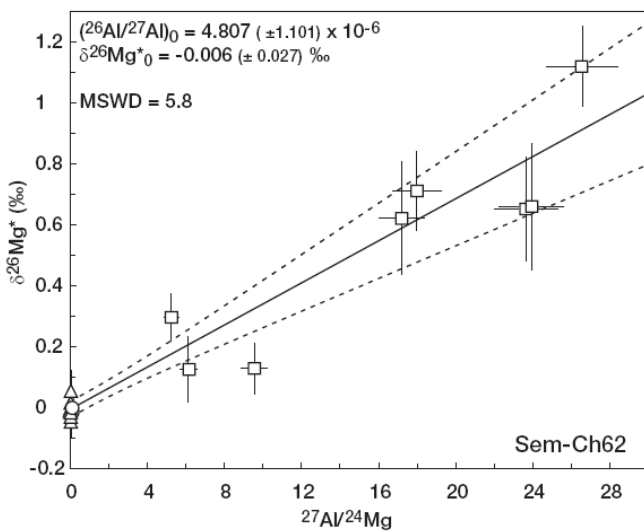
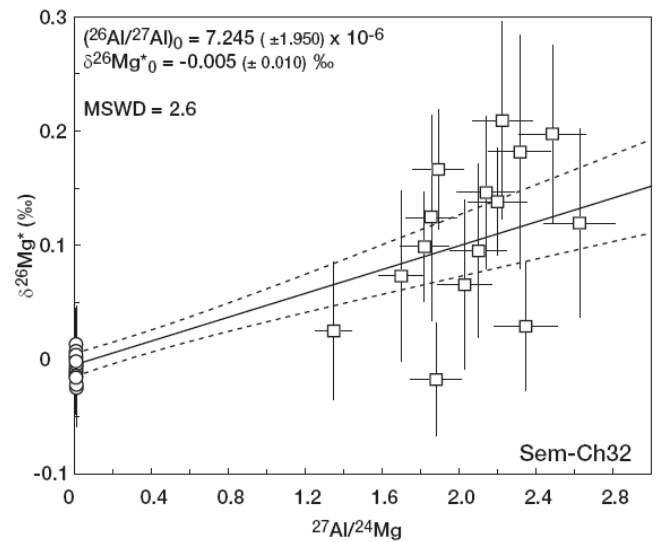
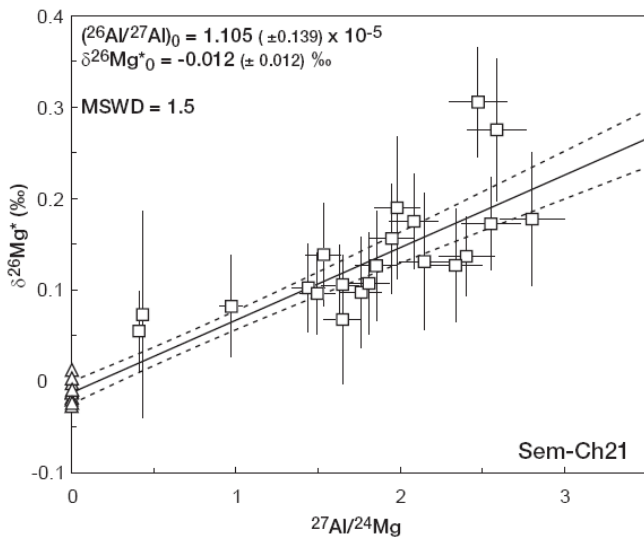
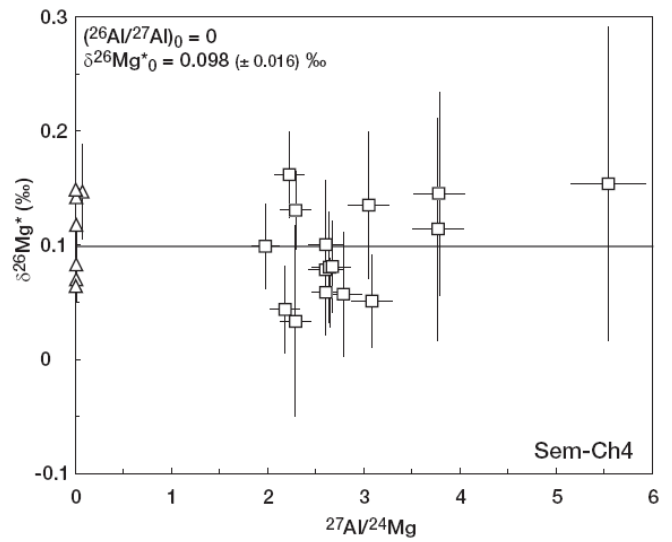
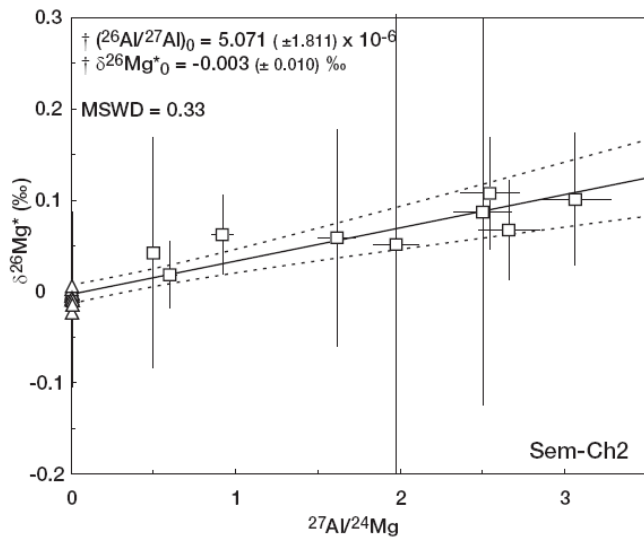
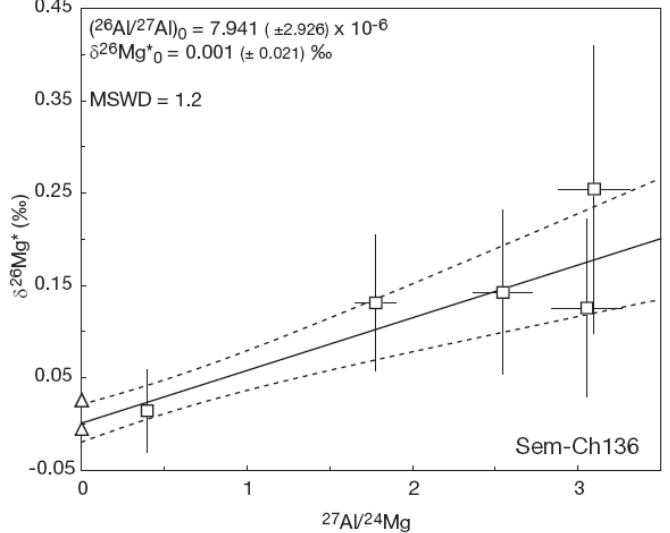
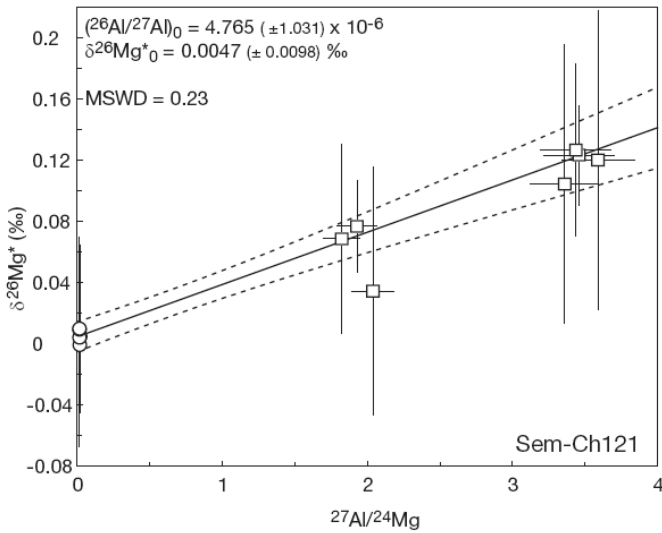
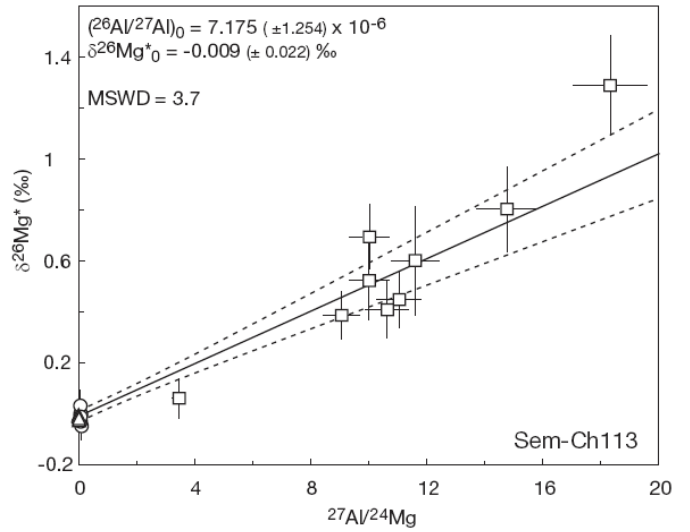
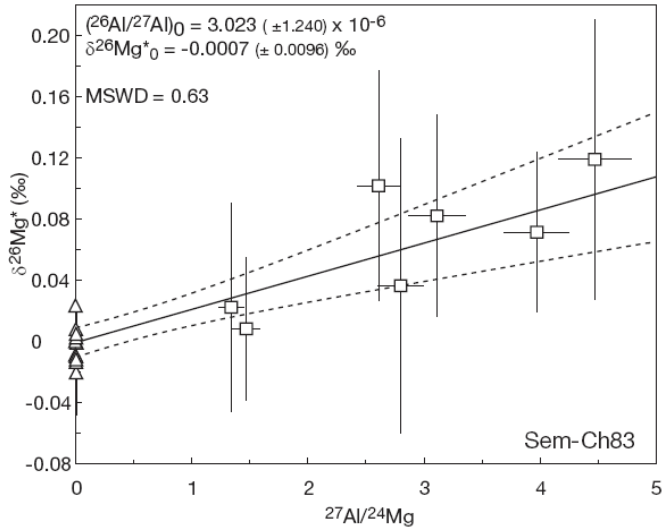
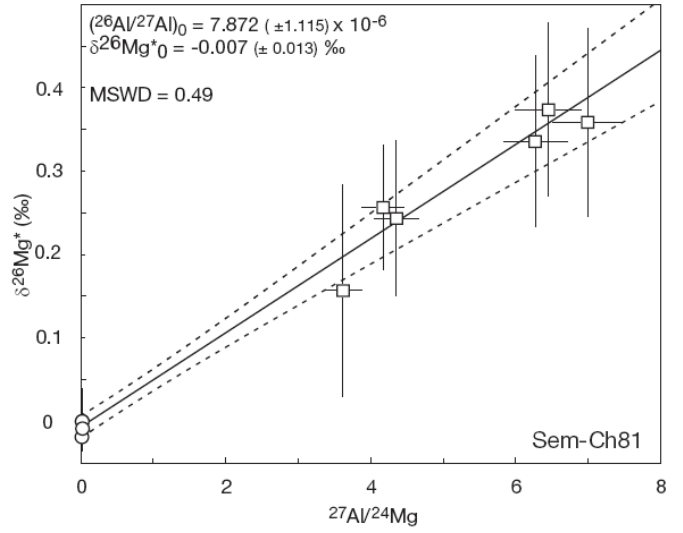
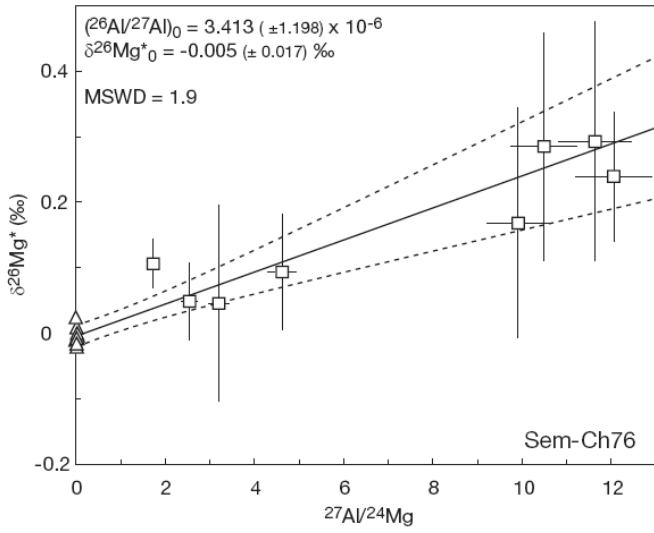


Fig. S3: $\delta^{25}\text{Mg}$ values measured in chondrules, corrected at first order for instrumental mass fractionation determined for terrestrial standards of olivine, low-Ca pyroxene and glass (Fig. S2). Data are not precisely corrected for variations in instrumental mass fractionation due to variations in chemical composition (matrix effect). This could explain the range of variations of ± 1 ‰ observed in olivine and pyroxene. The negative values up to -3 ‰ in mesostasis correspond to analyses performed both in glass (instrumental mass fractionation at about $+3$ ‰ to $+5$ ‰ in terrestrial standards) and dendritic crystals of high-Ca pyroxene (instrumental mass fractionation closes to 0 ‰ in terrestrial standards). Two sigma error bars.





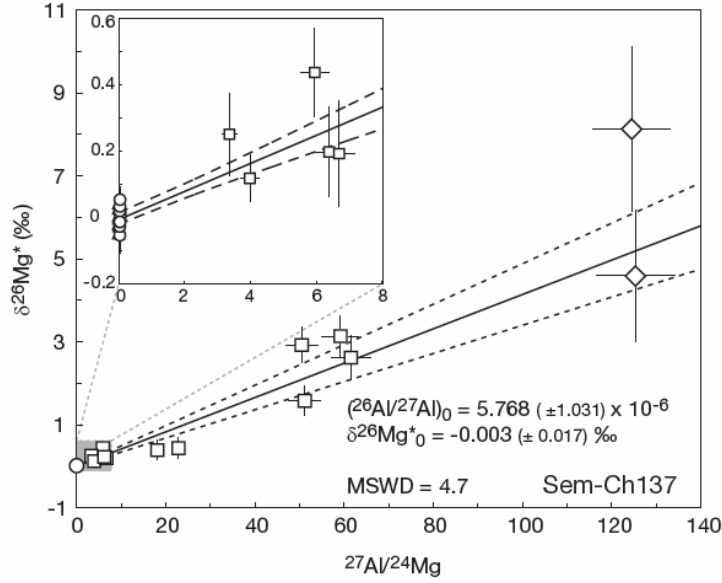


Fig. S3: Isochron diagrams obtained from ion probe analyses for the fifteen Semarkona chondrules (open circles are for low-Ca pyroxene, open triangles for olivine, open square for mesostasis and open diamonds for plagioclase). Two sigma error bars.

† For type I Sem-Ch2, as mentioned in the text, if the Mg-rich olivines did not crystallized from the melt corresponding to the quench mesostasis, then in theory the olivines must not be included in the calculation of the isochron to date chondrule melting. An isochron calculated without olivine data gave a $(^{26}\text{Al}/^{27}\text{Al})_0$ of $3.901 (\pm 2.926) \times 10^{-6}$ and a poorly constrained $\delta^{26}\text{Mg}^*_0$ of $0.016 (\pm 0.038) \text{‰}$. Thus it is not possible to determine a precise isochron only with the mesostasis. However, using the solar nebula growth curve, the $(^{26}\text{Al}/^{27}\text{Al})_0$ would give a $\delta^{26}\text{Mg}^*$ for the hypothetical olivine in equilibrium with the mesostasis of $\approx -0.005 \text{‰}$. If considering this value as the value for olivine crystallized at equilibrium from Sem-Ch2 melt, it is possible to recalculate by iteration an isochron with a good precision with a $(^{26}\text{Al}/^{27}\text{Al})_0$ of $5.057 (\pm 1.811) \times 10^{-6}$ and a $\delta^{26}\text{Mg}^*_0$ of $-0.0029 (\pm 0.012) \text{‰}$. This isochron is the same as the complete one calculated with the olivine data given in Table 1. Varying the $\delta^{26}\text{Mg}^*$ of these theoretical olivines does not change significantly the $(^{26}\text{Al}/^{27}\text{Al})_0$. This indicates that if the olivines are relicts, they formed closely before the chondrule (at the time resolution given by the ^{26}Al - ^{26}Mg chronometer and the precision of our data)

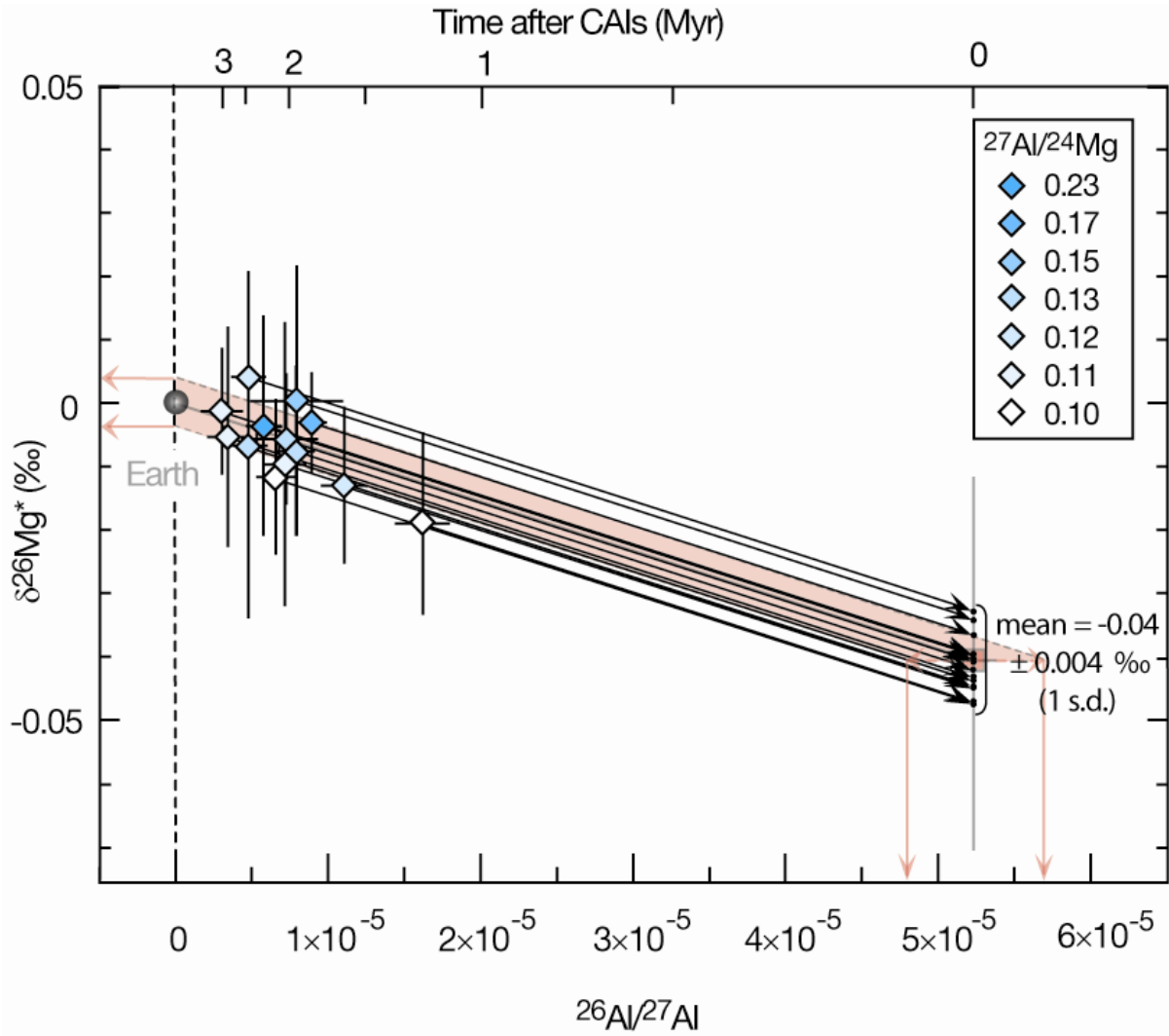


Fig. S5: Method used to calculate the relative heterogeneity of $\approx \pm 10\%$, i.e. $\pm 0.5 \times 10^{-5}$ for $^{26}\text{Al}/^{27}\text{Al}$ ratios and $\pm 0.004 \text{ ‰}$ for $\delta^{26}\text{Mg}^*$:

- (i) We assumed that all the variability in chondrules compositions [$(^{26}\text{Al}/^{27}\text{Al})_0$ and $\delta^{26}\text{Mg}^*_0$] is due to initial ^{26}Al heterogeneity, i.e. these chondrules come from gas with heterogeneous $^{26}\text{Al}/^{27}\text{Al}$ compositions.
- (ii) We determined the growth curve by reverse path for each chondrule using the chondritic $^{27}\text{Al}/^{24}\text{Mg}$ ratio (black lines), in order to find the $\delta^{26}\text{Mg}^*$ of the gas from which they come from, at the time of formation of CAIs, i.e. when $^{26}\text{Al}/^{27}\text{Al}$ ratio was 5.25×10^{-5} (black points).
- (iii) We calculated the mean and the standard deviation of these $\delta^{26}\text{Mg}^*$ (-0.04 ‰ and $\pm 0.004 \text{ ‰}$) that gave the heterogeneity of $\delta^{26}\text{Mg}^*$ at the time of formation of CAIs.
- (iv) Finally, we calculated the growth curves considering the two extreme $\delta^{26}\text{Mg}^*$ values (-0.044 and -0.036) and we determined the heterogeneity of the $^{26}\text{Al}/^{27}\text{Al}$ ratio of the gas at the time of formation of CAIs ($\pm 0.5 \times 10^{-5}$) for $\delta^{26}\text{Mg}^* = -0.04 \text{ ‰}$.

3. Supporting tables

Chondrule	Phase	$^{27}\text{Al}/^{24}\text{Mg}$	$\delta^{26}\text{Mg}^*$ (‰)	$(^{27}\text{Al}/^{26}\text{Al})_0$ Age after CAIs $\delta^{26}\text{Mg}^*_0$ (‰)	Bulk $^{27}\text{Al}/^{24}\text{Mg}$
Sem-Ch2					
1	Olivine	3.6×10^{-3}	-0.023 ± 0.048		
2	Mesostasis	1.976	0.052 ± 0.252		
3	Mesostasis	0.922	0.062 ± 0.044		
4	Mesostasis	0.499	0.042 ± 0.126		
5	Mesostasis	2.503	0.087 ± 0.211		
6	Olivine	7.1×10^{-3}	-0.009 ± 0.095		
7	Olivine	8.5×10^{-3}	-0.004 ± 0.047		
8	Olivine	1.0×10^{-3}	0.009 ± 0.09	$(5.071 \pm 1.811) \times 10^{-6}$	
9	Olivine	2.0×10^{-3}	-0.033 ± 0.124		
10	Olivine	1.0×10^{-3}	-0.002 ± 0.048		
11	Olivine	3.0×10^{-3}	-0.024 ± 0.066	$^{+0.465}$ 2.457 Myr	0.13
12	Olivine	2.0×10^{-3}	0.008 ± 0.043	$^{-0.312}$	
13	Olivine	4.0×10^{-3}	-0.009 ± 0.054		
14	Olivine	2.4×10^{-3}	-0.011 ± 0.038		
15	Olivine	1.5×10^{-3}	0.004 ± 0.022	-0.003 ± 0.010	
16	Mesostasis	2.545	0.108 ± 0.061		
17	Mesostasis	1.616	0.059 ± 0.119		
18	Mesostasis	2.660	0.067 ± 0.054		
19	Olivine	3.2×10^{-3}	-0.002 ± 0.023		
20	Mesostasis	3.065	0.101 ± 0.072		
21	Mesostasis	0.599	0.018 ± 0.036		
22	Olivine	5.2×10^{-3}	-0.017 ± 0.037		
Sem-Ch4					
1	Olivine	1.9×10^{-2}	0.087 ± 0.035		
2	Olivine	7.8×10^{-2}	0.147 ± 0.041		
3	Olivine	9.1×10^{-3}	0.072 ± 0.025		
4	Mesostasis	2.291	0.033 ± 0.083		
5	Mesostasis	3.769	0.114 ± 0.097		
6	Mesostasis	5.542	0.154 ± 0.137		
7	Mesostasis	3.785	0.145 ± 0.089	0	
8	Olivine	9.9×10^{-3}	0.067 ± 0.051		0.70
9	Mesostasis	2.604	0.079 ± 0.057	0.098 ± 0.016	
10	Mesostasis	2.182	0.044 ± 0.038		
11	Mesostasis	2.649	0.059 ± 0.03		
12	Mesostasis	2.641	0.08 ± 0.048		
13	Mesostasis	2.608	0.1 ± 0.056		
14	Olivine	6.7×10^{-3}	0.128 ± 0.032		
15	Mesostasis	3.084	0.051 ± 0.04		
16	Mesostasis	2.789	0.057 ± 0.054		

Chondrule	Phase	$^{27}\text{Al}/^{24}\text{Mg}$	$\delta^{26}\text{Mg}^*$ (‰)	$(^{27}\text{Al}/^{26}\text{Al})_0$ Age after CAIs $\delta^{26}\text{Mg}^*_0$ (‰)	Bulk $^{27}\text{Al}/^{24}\text{Mg}$
17	Mesostasis	3.052	0.135 ± 0.064		
18	Mesostasis	2.226	0.162 ± 0.037		
19	Olivine	7.1×10^{-3}	0.108 ± 0.021		
20	Mesostasis	2.671	0.081 ± 0.04		
21	Mesostasis	1.978	0.099 ± 0.037		
22	Olivine	7.4×10^{-3}	0.138 ± 0.027		
23	Mesostasis	2.292	0.131 ± 0.034		
Sem-Ch21					
1	Mesostasis	2.804	0.178 ± 0.073		
2	Mesostasis	1.855	0.126 ± 0.06		
3	Mesostasis	2.404	0.137 ± 0.044		
4	Mesostasis	2.589	0.275 ± 0.078		
5	Mesostasis	0.409	0.055 ± 0.044		
6	Mesostasis	2.552	0.172 ± 0.05		
7	Mesostasis	1.982	0.19 ± 0.078		
8	Olivine	9.8×10^{-4}	-0.015 ± 0.027		
9	Mesostasis	0.972	0.082 ± 0.055		
10	Mesostasis	1.649	0.068 ± 0.07		
11	Mesostasis	2.338	0.127 ± 0.062		
12	Mesostasis	2.084	0.175 ± 0.052		
13	Olivine	3.0×10^{-4}	-0.005 ± 0.08	$(1.105 \pm 0.139) \times 10^{-5}$	
14	Olivine	3.0×10^{-4}	0.006 ± 0.065		
15	Mesostasis	1.440	0.102 ± 0.049		
16	Olivine	2.3×10^{-4}	-0.02 ± 0.05	$^{+0.142}$ 1.637 Myr	0.12
17	Mesostasis	0.431	0.073 ± 0.113	$^{-0.125}$	
18	Olivine	3.8×10^{-4}	0.012 ± 0.082		
19	Olivine	4.5×10^{-4}	-0.014 ± 0.044		
20	Olivine	3.1×10^{-4}	-0.034 ± 0.04	-0.012 ± 0.012	
21	Mesostasis	2.148	0.131 ± 0.075		
22	Mesostasis	1.495	0.096 ± 0.044		
23	Mesostasis	1.634	0.105 ± 0.043		
24	Olivine	5.4×10^{-4}	-0.025 ± 0.022		
25	Mesostasis	1.764	0.098 ± 0.06		
26	Olivine	2.9×10^{-4}	-0.018 ± 0.02		
27	Olivine	3.0×10^{-4}	0.002 ± 0.026		
28	Mesostasis	1.810	0.107 ± 0.055		
29	Mesostasis	1.949	0.156 ± 0.06		
30	Mesostasis	1.534	0.139 ± 0.056		
31	Olivine	3.1×10^{-4}	0.026 ± 0.045		
32	Mesostasis	2.475	0.306 ± 0.06		

Chondrule	Phase	$^{27}\text{Al}/^{24}\text{Mg}$	$\delta^{26}\text{Mg}^*$ (‰)	$(^{27}\text{Al}/^{26}\text{Al})_0$ Age after CAIs $\delta^{26}\text{Mg}^*_0$ (‰)	Bulk $^{27}\text{Al}/^{24}\text{Mg}$
Sem-Ch32					
1	Orthopyroxene	8.3×10^{-3}	-0.006 ± 0.053		
2	Mesostasis	2.485	0.197 ± 0.078		
3	Mesostasis	2.225	0.209 ± 0.086		
4	Mesostasis	1.892	0.167 ± 0.052		
5	Mesostasis	2.140	0.146 ± 0.067		
6	Orthopyroxene	1.0×10^{-2}	-0.009 ± 0.026		
7	Mesostasis	2.101	0.095 ± 0.076		
8	Mesostasis	1.880	-0.018 ± 0.05		
9	Mesostasis	1.347	0.025 ± 0.06		
10	Mesostasis	2.199	0.138 ± 0.047		
11	Mesostasis	2.346	0.029 ± 0.057	$(7.245 \pm 1.950) \times 10^{-6}$	
12	Orthopyroxene	9.0×10^{-3}	0.008 ± 0.017		
13	Orthopyroxene	8.0×10^{-3}	0.009 ± 0.027		
14	Orthopyroxene	6.0×10^{-3}	0.003 ± 0.017		
15	Orthopyroxene	8.0×10^{-3}	-0.002 ± 0.019	$2.081^{+0.330}_{-0.251}$ Myr	0.13
16	Orthopyroxene	7.0×10^{-3}	-0.012 ± 0.027		
17	Orthopyroxene	6.0×10^{-3}	-0.019 ± 0.018		
18	Orthopyroxene	9.0×10^{-3}	0.01 ± 0.022	-0.005 ± 0.010	
19	Orthopyroxene	6.1×10^{-3}	-0.021 ± 0.027		
20	Orthopyroxene	8.7×10^{-3}	-0.008 ± 0.025		
21	Mesostasis	1.699	0.073 ± 0.075		
22	Mesostasis	2.316	0.182 ± 0.102		
23	Orthopyroxene	7.8×10^{-3}	-0.014 ± 0.028		
24	Mesostasis	2.029	0.065 ± 0.074		
25	Mesostasis	1.819	0.099 ± 0.048		
26	Orthopyroxene	7.1×10^{-3}	0.018 ± 0.027		
27	Mesostasis	1.856	0.124 ± 0.09		
28	Mesostasis	2.626	0.119 ± 0.082		
29	Orthopyroxene	8.8×10^{-3}	-0.026 ± 0.022		
Sem-Ch62					
1	Olivine	2.1×10^{-4}	-0.032 ± 0.034		
2	Orthopyroxene	6.0×10^{-2}	0.009 ± 0.11	$(4.807 \pm 1.101) \times 10^{-6}$	
3	Olivine	2.2×10^{-4}	0.05 ± 0.028		
4	Mesostasis	23.964	0.659 ± 0.208		
5	Mesostasis	17.203	0.622 ± 0.186	$2513^{+0.274}_{-0.217}$ Myr	0.11
6	Olivine	2.8×10^{-4}	0.017 ± 0.02		
7	Mesostasis	23.653	0.651 ± 0.17	-0.006 ± 0.027	
8	Olivine	2.9×10^{-4}	-0.015 ± 0.035		
9	Mesostasis	9.553	0.127 ± 0.083		

Chondrule	Phase	$^{27}\text{Al}/^{24}\text{Mg}$	$\delta^{26}\text{Mg}^*$ (‰)	$(^{27}\text{Al}/^{26}\text{Al})_0$ Age after CAIs $\delta^{26}\text{Mg}^*_0$ (‰)	Bulk $^{27}\text{Al}/^{24}\text{Mg}$
10	Orthopyroxene	2.3×10^{-2}	-0.025 ± 0.027		
11	Mesostasis	26.585	1.119 ± 0.132		
12	Olivine	2.9×10^{-4}	-0.002 ± 0.042		
13	Mesostasis	5.233	0.295 ± 0.077		
14	Mesostasis	6.118	0.124 ± 0.108		
15	Mesostasis	17.992	0.71 ± 0.13		
16	Olivine	2.8×10^{-4}	-0.058 ± 0.036		
17	Olivine	2.6×10^{-4}	-0.04 ± 0.036		
Sem-Ch64					
1	Mesostasis	6.467	0.317 ± 0.179		
2	Mesostasis	5.620	0.369 ± 0.112		
3	Orthopyroxene	2.7×10^{-3}	-0.012 ± 0.033		
4	Orthopyroxene	2.6×10^{-3}	-0.027 ± 0.03		
5	Mesostasis	12.210	0.611 ± 0.25		
6	Orthopyroxene	7.1×10^{-3}	-0.014 ± 0.024		
7	Mesostasis	7.473	0.226 ± 0.179		
8	Orthopyroxene	7.5×10^{-3}	-0.011 ± 0.028		
9	Orthopyroxene	2.6×10^{-3}	-0.003 ± 0.026		
10	Orthopyroxene	2.9×10^{-3}	0.009 ± 0.024		
11	Orthopyroxene	8.5×10^{-3}	0.024 ± 0.027		
12	Mesostasis	10.504	0.605 ± 0.211	$(6.562 \pm 1.184) \times 10^{-6}$	
13	Mesostasis	10.026	0.48 ± 0.269		
14	Mesostasis	12.014	0.466 ± 0.245		
15	Mesostasis	10.946	0.539 ± 0.196		
16	Orthopyroxene	2.1×10^{-3}	-0.04 ± 0.035	$2.186^{+0.210}_{-0.174}$ Myr	0.10
17	Mesostasis	2.224	0.106 ± 0.089		
18	Mesostasis	12.097	0.688 ± 0.266		
19	Mesostasis	10.469	0.234 ± 0.223	-0.011 ± 0.012	
20	Mesostasis	6.936	0.229 ± 0.213		
21	Mesostasis	31.205	1.401 ± 0.604		
22	Orthopyroxene	2.6×10^{-2}	-0.049 ± 0.024		
23	Orthopyroxene	2.1×10^{-3}	-0.021 ± 0.032		
24	Mesostasis	16.731	0.573 ± 0.298		
25	Mesostasis	9.158	0.527 ± 0.279		
26	Orthopyroxene	1.7×10^{-2}	-0.077 ± 0.03		
27	Orthopyroxene	2.4×10^{-3}	0.004 ± 0.034		
28	Mesostasis	14.072	0.44 ± 0.157		
29	Mesostasis	12.063	0.853 ± 0.193		
30	Orthopyroxene	2.3×10^{-3}	-0.005 ± 0.037		
31	Orthopyroxene	2.1×10^{-3}	0.017 ± 0.023		

Chondrule	Phase	$^{27}\text{Al}/^{24}\text{Mg}$	$\delta^{26}\text{Mg}^*$ (‰)	$(^{27}\text{Al}/^{26}\text{Al})_0$ Age after CAIs $\delta^{26}\text{Mg}^*_0$ (‰)	Bulk $^{27}\text{Al}/^{24}\text{Mg}$
32	Orthopyroxene	2.5×10^{-3}	-0.014 ± 0.036		
33	Mesostasis	5.063	0.417 ± 0.213		
34	Orthopyroxene	3.2×10^{-3}	-0.034 ± 0.037		
35	Orthopyroxene	2.0×10^{-3}	0.01 ± 0.021		
Sem-Ch76					
1	Olivine	9.2×10^{-4}	-0.043 ± 0.128		
2	Mesostasis	10.490	0.285 ± 0.174		
3	Mesostasis	1.732	0.106 ± 0.037		
4	Mesostasis	11.636	0.292 ± 0.182		
5	Olivine	3.2×10^{-4}	-0.039 ± 0.1		
6	Mesostasis	9.912	0.168 ± 0.175	$(3.413 \pm 1.198) \times 10^{-6}$	
7	Mesostasis	3.202	0.045 ± 0.15		
8	Olivine	4.0×10^{-4}	-0.003 ± 0.087		
9	Olivine	6.4×10^{-4}	-0.024 ± 0.031	$2.874^{+0.455}_{-0.317}$ Myr	0.11
10	Olivine	8.5×10^{-4}	-0.008 ± 0.032		
11	Olivine	3.6×10^{-4}	-0.042 ± 0.029		
12	Mesostasis	4.618	0.093 ± 0.087		
13	Olivine	3.8×10^{-4}	0.019 ± 0.027	-0.005 ± 0.017	
14	Mesostasis	2.542	0.049 ± 0.059		
15	Olivine	4.3×10^{-4}	-0.001 ± 0.034		
16	Mesostasis	12.054	0.239 ± 0.098		
17	Olivine	4.8×10^{-4}	-0.025 ± 0.034		
18	Olivine	3.3×10^{-4}	0.022 ± 0.04		
Sem-Ch81					
1	Mesostasis	4.172	0.256 ± 0.075		
2	Mesostasis	4.356	0.243 ± 0.093		
3	Mesostasis	6.271	0.335 ± 0.103	$(7.872 \pm 1.115) \times 10^{-6}$	
4	Mesostasis	6.995	0.359 ± 0.113		
5	Mesostasis	6.455	0.374 ± 0.104	$1.994^{+0.161}_{-0.139}$ Myr	0.13
6	Orthopyroxene	4.9×10^{-3}	-0.022 ± 0.026		
7	Orthopyroxene	3.8×10^{-3}	-0.013 ± 0.035		
8	Orthopyroxene	6.2×10^{-3}	0.003 ± 0.02	-0.007 ± 0.013	
9	Mesostasis	3.620	0.157 ± 0.127		
10	Orthopyroxene	1.5×10^{-2}	0.002 ± 0.038		
Sem-Ch83					
1	Olivine	6.4×10^{-4}	-0.021 ± 0.032		
2	Olivine	7.2×10^{-4}	0.015 ± 0.028	$(3.023 \pm 1.240) \times 10^{-6}$	
3	Mesostasis	3.113	0.082 ± 0.066		0.11
4	Mesostasis	1.468	0.008 ± 0.047		

Chondrule	Phase	$^{27}\text{Al}/^{24}\text{Mg}$	$\delta^{26}\text{Mg}^*$ (‰)	$(^{27}\text{Al}/^{26}\text{Al})_0$ Age after CAIs $\delta^{26}\text{Mg}^*_0$ (‰)	Bulk $^{27}\text{Al}/^{24}\text{Mg}$
5	Mesostasis	1.338	0.022 ± 0.068		
6	Olivine	1.0×10^{-3}	0.011 ± 0.047		
7	Olivine	6.2×10^{-4}	0.005 ± 0.056		
8	Olivine	5.2×10^{-4}	-0.004 ± 0.018		
9	Olivine	6.1×10^{-4}	-0.004 ± 0.065		
10	Olivine	6.3×10^{-4}	0.007 ± 0.029	$3.002^{+0.555}_{-0.362}$ Myr	
11	Mesostasis	4.473	0.119 ± 0.092		
12	Mesostasis	3.974	0.071 ± 0.052		
13	Olivine	1.6×10^{-3}	-0.013 ± 0.035		
14	Mesostasis	2.798	0.036 ± 0.097	-0.0007 ± 0.0096	
15	Mesostasis	2.609	0.102 ± 0.075		
16	Olivine	1.0×10^{-3}	0.024 ± 0.035		
17	Olivine	7.4×10^{-4}	-0.004 ± 0.054		
18	Olivine	5.3×10^{-4}	-0.015 ± 0.04		
Sem-Ch113					
1	Olivine	7.0×10^{-4}	-0.033 ± 0.037		
2	Olivine	6.1×10^{-4}	-0.004 ± 0.043		
3	Olivine	3.3×10^{-4}	0.013 ± 0.031		
4	Mesostasis	9.055	0.386 ± 0.093		
5	Mesostasis	18.318	1.289 ± 0.194		
6	Mesostasis	10.012	0.694 ± 0.128		
7	Mesostasis	14.759	0.803 ± 0.167	$(7.175 \pm 1.254) \times 10^{-6}$	
8	Mesostasis	10.005	0.523 ± 0.156		
9	Mesostasis	11.599	0.601 ± 0.213		
10	Orthopyroxene	1.5×10^{-2}	0.037 ± 0.056	$2.092^{+0.202}_{-0.170}$ Myr	0.11
11	Mesostasis	11.037	0.45 ± 0.111		
12	Mesostasis	3.454	0.061 ± 0.078		
13	Mesostasis	10.632	0.408 ± 0.113		
14	Orthopyroxene	2.0×10^{-2}	-0.013 ± 0.032	-0.009 ± 0.022	
15	Orthopyroxene	8.0×10^{-2}	-0.066 ± 0.037		
16	Orthopyroxene	4.4×10^{-2}	0.003 ± 0.028		
17	Olivine	6.2×10^{-4}	-0.023 ± 0.031		
18	Olivine	2.6×10^{-3}	-0.006 ± 0.049		
19	Orthopyroxene	4.3×10^{-2}	0.002 ± 0.061		
20	Orthopyroxene	2.4×10^{-2}	0.046 ± 0.035		
Sem-Ch114					
1	Mesostasis	12.124	0.738 ± 0.135		
2	Mesostasis	14.701	1.044 ± 0.19	$(8.916 \pm 0.906) \times 10^{-6}$	
3	Mesostasis	13.867	0.787 ± 0.194		0.17
4	Mesostasis	11.965	0.848 ± 0.184		
5	Olivine	3.5×10^{-4}	-0.006 ± 0.025		

Chondrule	Phase	$^{27}\text{Al}/^{24}\text{Mg}$	$\delta^{26}\text{Mg}^*$ (‰)	$(^{27}\text{Al}/^{26}\text{Al})_0$ Age after CAIs $\delta^{26}\text{Mg}^*_0$ (‰)	Bulk $^{27}\text{Al}/^{24}\text{Mg}$	Chondrule	Phase	$^{27}\text{Al}/^{24}\text{Mg}$	$\delta^{26}\text{Mg}^*$ (‰)	$(^{27}\text{Al}/^{26}\text{Al})_0$ Age after CAIs $\delta^{26}\text{Mg}^*_0$ (‰)	Bulk $^{27}\text{Al}/^{24}\text{Mg}$
6	Olivine	3.5×10^{-4}	-0.007 ± 0.037			10	Mesostasis	6.387	0.198 ± 0.135		
7	Mesostasis	7.731	0.456 ± 0.133			11	Mesostasis	5.949	0.438 ± 0.132		
8	Olivine	3.3×10^{-4}	0.003 ± 0.03	$^{+0.113}$		12	Orthopyroxene	4.1×10^{-2}	0.016 ± 0.03		
9	Orthopyroxene	3.0×10^{-3}	0.003 ± 0.024	1.863	Myr	13	Orthopyroxene	3.5×10^{-2}	-0.006 ± 0.032		
10	Orthopyroxene	2.0×10^{-3}	0.016 ± 0.033			14	Orthopyroxene	3.9×10^{-2}	0.062 ± 0.029		
11	Orthopyroxene	2.5×10^{-3}	0.01 ± 0.019			15	Orthopyroxene	4.7×10^{-2}	0.008 ± 0.026		
12	Orthopyroxene	3.2×10^{-3}	-0.011 ± 0.026	-0.0024 ± 0.0075		16	Mesostasis	50.509	2.921 ± 0.432		
13	Olivine	3.0×10^{-4}	-0.005 ± 0.023			17	Mesostasis	59.213	3.136 ± 0.481		
14	Olivine	3.0×10^{-4}	-0.011 ± 0.015			18	Mesostasis	61.557	2.62 ± 0.53		
Sem-Ch121						19	Olivine	5.7×10^{-4}	-0.023 ± 0.025	$^{+0.207}$	
1	Mesostasis	3.590	0.12 ± 0.098			20	Olivine	6.3×10^{-4}	0.027 ± 0.046	2.322	Myr
2	Orthopyroxene	1.3×10^{-2}	0.001 ± 0.069			21	Olivine	2.2×10^{-3}	0.049 ± 0.039	$^{-0.173}$	
3	Orthopyroxene	2.3×10^{-2}	0.01 ± 0.055	$(4.765 \pm 1.031) \times 10^{-6}$		22	Plagioclase	124.531	8.13 ± 1.983		
4	Mesostasis	1.824	0.069 ± 0.062			23	Plagioclase	125.446	4.592 ± 1.595	-0.003 ± 0.017	
5	Mesostasis	3.360	0.105 ± 0.091			24	Mesostasis	3.360	0.251 ± 0.124		
6	Mesostasis	2.039	0.035 ± 0.081	$^{+0.257}$		25	Orthopyroxene	1.6×10^{-3}	-0.006 ± 0.033		
7	Orthopyroxene	1.8×10^{-2}	0.011 ± 0.016	2.523	Myr	26	Orthopyroxene	2.4×10^{-2}	-0.032 ± 0.048		
8	Orthopyroxene	2.3×10^{-2}	0.004 ± 0.02	$^{-0.206}$		27	Orthopyroxene	3.8×10^{-2}	0.026 ± 0.04		
9	Mesostasis	1.928	0.077 ± 0.03			28	Olivine	6.1×10^{-4}	-0.016 ± 0.053		
10	Mesostasis	3.459	0.124 ± 0.033	0.0047 ± 0.0098	0.12	29	Olivine	8.7×10^{-4}	-0.008 ± 0.045		
11	Mesostasis	3.438	0.127 ± 0.056			30	Mesostasis	6.688	0.193 ± 0.161		
12	Orthopyroxene	1.1×10^{-2}	-0.001 ± 0.018			31	Orthopyroxene	3.4×10^{-2}	0.019 ± 0.046		
Sem-Ch136						32	Orthopyroxene	4.2×10^{-2}	0.011 ± 0.043		
1	Olivine	1.9×10^{-3}	-0.019 ± 0.03			Sem-Ch138					
2	Mesostasis	3.054	0.125 ± 0.096	$(7.941 \pm 2.926) \times 10^{-6}$		1	Orthopyroxene	2.0×10^{-3}	-0.021 ± 0.035		
3	Mesostasis	0.397	0.014 ± 0.045			2	Orthopyroxene	2.2×10^{-3}	-0.029 ± 0.067		
4	Mesostasis	3.098	0.254 ± 0.156	$^{+0.484}$		3	Mesostasis	4.461	0.46 ± 0.201		
5	Mesostasis	2.547	0.143 ± 0.089	1.985	Myr	4	Orthopyroxene	2.8×10^{-2}	-0.022 ± 0.045		
6	Olivine	1.5×10^{-3}	0.03 ± 0.057	$^{-0.330}$		5	Mesostasis	2.927	0.316 ± 0.15	$(1.619 \pm 0.167) \times 10^{-5}$	
7	Mesostasis	1.778	0.131 ± 0.074	0.001 ± 0.021	0.15	6	Mesostasis	2.476	0.386 ± 0.185		
8	Olivine	1.3×10^{-3}	0.03 ± 0.045			7	Mesostasis	4.479	0.335 ± 0.283		
Sem-Ch137						8	Mesostasis	4.568	0.467 ± 0.191	$^{+0.115}$	
1	Orthopyroxene	3.6×10^{-2}	-0.062 ± 0.045			9	Mesostasis	2.792	0.388 ± 0.151	1.235	Myr
2	Olivine	6.7×10^{-4}	-0.027 ± 0.029			10	Mesostasis	0.260	0.033 ± 0.084	$^{-0.104}$	
3	Mesostasis	18.151	0.387 ± 0.231			11	Mesostasis	2.999	0.334 ± 0.079		
4	Mesostasis	22.883	0.436 ± 0.244	$(5.768 \pm 1.031) \times 10^{-6}$		12	Mesostasis	4.554	0.468 ± 0.126		
5	Mesostasis	51.203	1.575 ± 0.356			13	Mesostasis	3.851	0.444 ± 0.068	-0.018 ± 0.014	
6	Orthopyroxene	4.6×10^{-2}	0.012 ± 0.046		0.23	14	Orthopyroxene	2.1×10^{-3}	-0.011 ± 0.043		
7	Olivine	1.1×10^{-3}	-0.006 ± 0.034			15	Orthopyroxene	2.5×10^{-3}	-0.006 ± 0.041		
8	Mesostasis	3.982	0.118 ± 0.071			16	Orthopyroxene	1.9×10^{-3}	0.017 ± 0.044		
9	Olivine	6.0×10^{-4}	-0.053 ± 0.028			17	Orthopyroxene	2.2×10^{-3}	-0.036 ± 0.046		
						18	Orthopyroxene	2.8×10^{-3}	-0.035 ± 0.03		

Table S1: Al and Mg isotopic compositions for each measurement within the fifteen studied chondrules. $(^{26}\text{Al}/^{27}\text{Al})_0$ and $\delta^{26}\text{Mg}^*_0$ were inferred for each chondrule from the classical error-weighted regression model 1 of Isoplot 3.00 (SI7). Errors on $^{27}\text{Al}/^{24}\text{Mg}$ ratios are $\pm 7\%$ relative (see Methods for details). Bulk $^{27}\text{Al}/^{24}\text{Mg}$ ratios were obtained by chemical mapping using the Cameca SX-100 electron microprobe at Université Henri Poincaré (Nancy, France). Errors are two sigma.

Chondrite	Class	Chondrule	type	$(^{26}\text{Al}/^{27}\text{Al})_0$	2σ error	Reference
Y81020	CO3.0	Y10	I	1.03×10^{-5}	2.80×10^{-6}	(S8)
Y81020	CO3.0	Y3	I	9.00×10^{-6}	2.80×10^{-6}	(S8)
Y81020	CO3.0	Y20	I	8.80×10^{-6}	6.40×10^{-6}	(S8)
Y81020	CO3.0	Y24	I	7.90×10^{-6}	1.20×10^{-6}	(S8)
Y81020	CO3.0	Y08	I	7.40×10^{-6}	2.10×10^{-6}	(S8)
Y81020	CO3.0	Y76	I	7.00×10^{-6}	2.00×10^{-6}	(S8)
Y81020	CO3.0	Y09	I	6.90×10^{-6}	2.00×10^{-6}	(S8)
Y81020	CO3.0	Y29	I	6.60×10^{-6}	1.20×10^{-6}	(S8)
Y81020	CO3.0	Y17	I	6.60×10^{-6}	3.50×10^{-6}	(S8)
Y81020	CO3.0	Y12	I	6.60×10^{-6}	1.90×10^{-6}	(S8)
Y81020	CO3.0	Y18	I	6.20×10^{-6}	1.90×10^{-6}	(S8)
Y81020	CO3.0	Y71	I	5.70×10^{-6}	1.50×10^{-6}	(S8)
Y81020	CO3.0	Y01	I	4.90×10^{-6}	1.40×10^{-6}	(S8)
Y81020	CO3.0	Y2-14	II	7.40×10^{-6}	4.20×10^{-6}	(S8)
Y81020	CO3.0	Y2-09	II	7.30×10^{-6}	1.10×10^{-6}	(S8)
Y81020	CO3.0	Y56	II	6.10×10^{-6}	1.50×10^{-6}	(S8)
Y81020	CO3.0	Y58	II	5.70×10^{-6}	2.90×10^{-6}	(S8)
Y81020	CO3.0	Y46	II	4.60×10^{-6}	1.80×10^{-6}	(S8)
Y81020	CO3.0	Y2-44	II	2.90×10^{-6}	9.00×10^{-7}	(S8)
Y81020	CO3.0	Y175	II	8.20×10^{-6}	1.20×10^{-6}	(S8)
Y81020	CO3.0	Y23	II	4.10×10^{-6}	1.10×10^{-6}	(S8)
Y81020	CO3.0	E3t	II PO	3.70×10^{-6}	1.10×10^{-6}	(S4)
Y81020	CO3.0	G4i	II PO	4.00×10^{-6}	1.90×10^{-6}	(S4)
Y81020	CO3.0	F7o	II PO	4.20×10^{-6}	1.30×10^{-6}	(S4)
Y81020	CO3.0	G7g	II PO	2.40×10^{-6}	1.70×10^{-6}	(S4)
Y81020	CO3.0	C6w	II PO	6.50×10^{-6}	3.20×10^{-6}	(S4)
Y81020	CO3.0		II PO	4.60×10^{-6}	3.00×10^{-6}	(S2)
Acfer 311	CR	PL20CHD2	I POP	3.20×10^{-6}	1.40×10^{-6}	(S6)
?	CR		II	2.20×10^{-6}	1.40×10^{-6}	(S5)
EET 92042	CR	Ch1	Al-rich	9.50×10^{-7}	2.90×10^{-7}	(S5)
EET 92147	CR	Ch1	Al-rich	6.20×10^{-6}	8.00×10^{-7}	(S5)
El Djouf 001	CR	MKCHD1	Al-rich	4.50×10^{-6}	1.10×10^{-6}	(S6)
El Djouf 001	CR	PL72CHD5	Al-rich	3.20×10^{-6}	1.30×10^{-6}	(S6)
Efremovka	CV3		I	5.60×10^{-6}	3.30×10^{-6}	(S1)
Ningqiang	Anom. CV	Chon-2	I BO	3.40×10^{-6}	2.10×10^{-6}	(S3)
Ningqiang	Anom. CV	Chon-1	I PO	6.40×10^{-6}	3.60×10^{-6}	(S3)
Acfer 094	Ungr. CC	CHD63	I PO	4.90×10^{-6}	1.79×10^{-5}	(S7)
Acfer 094	Ungr. CC	CHD101	I PO	1.70×10^{-6}	4.40×10^{-6}	(S7)
Acfer 094	Ungr. CC	CHD31	I POP	1.03×10^{-5}	7.40×10^{-6}	(S7)
Acfer 094	Ungr. CC	CHD27	I PP	2.40×10^{-6}	9.40×10^{-6}	(S7)
Acfer 094	Ungr. CC	CHD58	I PP	3.10×10^{-6}	8.50×10^{-6}	(S7)

Acfer 094	Ungr. CC	CHD60	I PP	6.00×10^{-6}	3.80×10^{-6}	(S7)
Acfer 094	Ungr. CC	CHD102	I PP	5.90×10^{-6}	1.01×10^{-5}	(S7)
Adrar-003	L/LL3.1	2	II PO	6.30×10^{-6}	4.00×10^{-6}	(S15)
Adrar-003	L/LL3.1	3	II PO	8.40×10^{-6}	7.80×10^{-6}	(S15)
LEW86134	L3.0	36	II PO	1.63×10^{-5}	7.20×10^{-6}	(S15)
LEW86134	L3.0	3	II POP	7.10×10^{-6}	5.40×10^{-6}	(S15)
LEW86134	L3.0	16	II PP	1.03×10^{-5}	4.20×10^{-6}	(S15)
QUE97008	L3.05	1A	II PO	9.90×10^{-6}	6.00×10^{-6}	(S15)
QUE97008	L3.05	1B	II PO	1.95×10^{-5}	7.60×10^{-6}	(S15)
QUE97008	L3.05	5	II PO	7.90×10^{-6}	3.60×10^{-6}	(S15)
QUE97008	L3.05	16	II POP	1.10×10^{-5}	9.20×10^{-6}	(S15)
LEW86018	L3.1	6	II PO	7.40×10^{-6}	2.00×10^{-6}	(S15)
LEW86018	L3.1	6A	II PO	6.50×10^{-6}	2.30×10^{-6}	(S15)
LEW86018	L3.1	24	II POP	6.70×10^{-6}	3.60×10^{-6}	(S15)
LEW86018	L3.1	33	II POP	7.60×10^{-6}	3.60×10^{-6}	(S15)
ALHA77176	L3.2	1	II POP	6.50×10^{-6}	5.80×10^{-6}	(S15)
ALHA77176	L3.2	14B	II POP	9.70×10^{-6}	7.10×10^{-6}	(S15)
Semarkona	LL3.0	CC3-2	I BO	2.40×10^{-5}	6.00×10^{-6}	(S11)
Semarkona	LL3.0	CH3	I POP	8.80×10^{-6}	3.10×10^{-6}	(S12)
Bishunpur	LL3.1	B2-C10	I POP	1.02×10^{-5}	5.40×10^{-6}	(S14)
Bishunpur	LL3.1	B2-C17	I PP	3.50×10^{-6}	4.80×10^{-6}	(S14)
Chainpur 1251	LL3.4	CC16-3	I BO	4.30×10^{-6}	1.50×10^{-6}	(S11)
Semarkona	LL3.0	CH36	II BOP	6.60×10^{-6}	1.90×10^{-6}	(S12)
Semarkona	LL3.0	CH4	II PO	9.00×10^{-6}	1.60×10^{-6}	(S12)
Semarkona	LL3.0	CC-1	II POP	7.70×10^{-6}	2.10×10^{-6}	(S9)
Semarkona	LL3.0	CH23	II POP	9.20×10^{-6}	5.00×10^{-6}	(S12)
Semarkona	LL3.0	CH60	II POP	5.70×10^{-6}	2.60×10^{-6}	(S12)
Semarkona	LL3.0	Ch20	II POP	1.10×10^{-5}	2.40×10^{-6}	(S16)
Semarkona	LL3.0	Ch21	II POP	1.15×10^{-5}	5.40×10^{-6}	(S16)
Semarkona	LL3.0	Ch2	II PP	5.50×10^{-6}	3.00×10^{-7}	(S16)
Semarkona	LL3.0	Ch36	IPP	1.24×10^{-5}	5.20×10^{-6}	(S16)
Bishunpur	LL3.1	Ch45	II PO	5.80×10^{-6}	3.10×10^{-6}	(S16)
Bishunpur	LL3.1	Ch61	II PO	5.80×10^{-6}	2.20×10^{-6}	(S16)
Krymka	LL3.1	K21	II PO	1.03×10^{-5}	1.50×10^{-6}	(S13)
Y-791324	LL3.1	Ch3	II PO	1.10×10^{-5}	1.00×10^{-5}	(S16)
Bishunpur	LL3.1	B1-C4	II POP	1.20×10^{-5}	2.40×10^{-6}	(S13)
Bishunpur	LL3.1	B1-C18	II POP	8.40×10^{-6}	3.90×10^{-6}	(S13)
Bishunpur	LL3.1	B1-C4	II POP	1.54×10^{-5}	7.50×10^{-6}	(S14)
Bishunpur	LL3.1	B1-C18	II POP	9.50×10^{-6}	8.90×10^{-6}	(S14)
Bishunpur	LL3.1	B2-C1	II POP	2.28×10^{-5}	7.30×10^{-6}	(S14)
Bishunpur	LL3.1	B2-C7	II POP	5.50×10^{-6}	8.40×10^{-6}	(S14)
Bishunpur	LL3.1	B2-C12	II POP	4.50×10^{-6}	2.10×10^{-6}	(S14)
Bishunpur	LL3.1	B2-C18	II POP	5.70×10^{-6}	2.00×10^{-6}	(S14)
Bishunpur	LL3.1	B2-C20	II POP	7.40×10^{-6}	5.70×10^{-6}	(S14)
Y-791324	LL3.1	Ch6	II POP	1.22×10^{-5}	5.20×10^{-6}	(S16)
Bishunpur	LL3.1	B1-C56	II PP	9.60×10^{-6}	9.00×10^{-7}	(S13)

Bishunpur	LL3.1	B1-C56	II PP	1.40×10^{-5}	6.50×10^{-6}	(S14)
Bishunpur	LL3.1	B2-C13	II PP	5.30×10^{-6}	7.00×10^{-6}	(S14)
Krymka	LL3.1	K27	II PP	6.10×10^{-6}	1.70×10^{-6}	(S13)
ALHA76004	LL3.3	Ch1	II POP	1.06×10^{-5}	3.30×10^{-6}	(S16)
ALHA76004	LL3.3	Ch2	II POP	1.15×10^{-5}	3.40×10^{-6}	(S16)
ALHA76004	LL3.3	Ch11	II POP	7.10×10^{-6}	2.00×10^{-6}	(S16)
ALHA76004	LL3.3	Ch31	II POP	1.14×10^{-5}	2.80×10^{-6}	(S16)
Inman 5652	LL3.3-3.6	CC1-1	Al rich	9.40×10^{-6}	6.30×10^{-6}	(S10)
Chainpur 1251	LL3.4	CC1-3	Al rich	7.90×10^{-6}	2.70×10^{-6}	(S10)

Table S2: Compilation of the ^{26}Al data obtained by ion probe analyses from previous studies used for the Fig. 3. Only data with well-define isochrons slopes, i.e. with well-define $(^{26}\text{Al}/^{27}\text{Al})_0$ and errors, are considered in the table. Errors are two sigma. Data are from (S1-S16).

4. Supporting references

- S1. I. D. Hutcheon, A. N. Krot, A. A. Ulyanov, *Lunar Planet. Sci.* **XXXI**, 1869 (2000).
S2. H. Yurimoto, J. T. Wasson, *Geochim. Cosmochim. Acta* **66**, 4355-4363 (2002).
S3. W. B. Hsu, G. R. Huss, G. J. Wasserburg, *Meteorit. Planet. Sci.* **38**, 35-48 (2003).
S4. T. Kunihiro, A. E. Rubin, K. D. McKeegan, J. T. Wasson, *Geochim. Cosmochim. Acta* **68**, 2947 (2004).
S5. K. Nagashima, A. N. Krot, M. Chaussidon, *Meteorit. Planet. Sci.* **42**, A115 (2007).
S6. K. Nagashima, A. N. Krot, G. R. Huss, *Lunar Planet. Sci.* **XXXIX**, 2224 (2008).
S7. N. Sugiura, A. N. Krot, *Meteorit. Planet. Sci.* **42**, 1183-1195 (2007).
S8. E. Kurahashi, N. T. Kita, H. Nagahara, Y. Morishita, *Geochim. Cosmochim. Acta* **72**, A504 (2008).
S9. I. D. Hutcheon, R. Hutchison, *Nature* **337**, 238 (1989).
S10. S. S. Russell, G. Srinivasan, G. R. Huss, G. J. Wasserburg, G. J. MacPherson, *Science* **273**, 757 (1996).
S11. S. S. Russell, G. R. Huss, G. J. MacPherson, G. J. Wasserburg, *Lunar Planet. Sci.* **XXVIII**, 1468 (1997).
S12. N. T. Kita, H. Nagahara, S. Togashi, Y. Morishita, *Geochim. Cosmochim. Acta* **64**, 3913 (2000).
S13. N. T. Kita *et al.*, *Lunar Planet. Sci.* **XXXVI**, 1750 (2005).
S14. S. Mostefaoui *et al.*, *Meteorit. Planet. Sci.* **37**, 421-438 (2002).
S15. N. G. Rudraswami, J. N. Goswami, *Earth and Planet. Sci. Lett.* **257**, 231-244, (2007).
S16. N. G. Rudraswami, J. N. Goswami, B. Chattopadhyay, S. K. Sengupta, A. P. Thapliyal, *Earth and Planet. Sci. Lett.* **274**, 93 (2008).
S17. K. R. Ludwig, Berkeley Geochronology Center, Special Publication N°4 (2003)